Journal of Micromechanics and Microengineering

ACCEPTED MANUSCRIPT

Biocompatible bonding of a rigid off-stoichiometry thiol-ene-epoxy polymer microfluidic cartridge to a biofunctionalized silicon biosensor

To cite this article before publication: Linda Sønstevold *et al* 2022 *J. Micromech. Microeng.* in press https://doi.org/10.1088/1361-6439/ac6ebf

IOP Publishing Journal Title
Journal **XX** (XXXX) XXXXXX https://doi.org/XXXX/XXXX

Biocompatible bonding of a rigid off-stoichiometry thiol-ene-epoxy polymer microfluidic cartridge to a biofunctionalized silicon biosensor

Linda Sønstevold[1], Mukesh Yadav[2], Nina Bjørk Arnfinnsdottir[2], Aina Kristin Herbjørnrød[1], Geir Uri Jensen[1], Astrid Aksnes[2], Michal Marek Mielnik[1]

[1]SINTEF Digital, Microsystems and Nanotechnology (MiNaLab), Gaustadalléen 23C, 0373 Oslo, Norway
[2]Department of Electronic Systems, Norwegian University of Science and Technology, O. S. Bragstads plass 2, 7034 Trondheim, Norway

Corresponding author
Name Linda Sønstevold
E-mail address **linda.sonstevold@sintef.no**
Postal address SINTEF Digital, Microsystems and Nanotechnology (MiNaLab), Gaustadalléen 23C, 0373 Oslo, Norway
Telephone number +47 93263487

Received xxxxxx
Accepted for publication xxxxxx
Published xxxxxx

Abstract

Attachment of biorecognition molecules prior to microfluidic packaging is advantageous for many silicon biosensor-based lab-on-a-chip devices. This necessitates biocompatible bonding of the microfluidic cartridge, which, due to thermal or chemical incompatibility, excludes standard microfabrication bonding techniques. Here, we demonstrate a novel processing approach for a commercially available, two-step curable polymer to obtain biocompatible UVA-bonding of polymer microfluidics to silicon biosensors. Biocompatibility is assessed by UVA-bonding to antibody-functionalized ring resonator sensors and performing antigen capture assays while optically monitoring the sensor response. The assessments indicate normal biological function of the antibodies after UVA-bonding with selective binding to the target antigen. The bonding strength between polymer and silicon chips (non-biofunctionalized and biofunctionalized) is determined in terms of static liquid pressure. Polymer microfluidic cartridges are stored for more than 18 weeks between cartridge molding and cartridge-to-silicon bonding. All bonded devices withstand more than 2500 mbar pressure, far exceeding the typical requirements for lab-on-a-chip applications, while they may also be de-bonded after use. We suggest that these characteristics arise from bonding mainly through intermolecular forces, with a large extent of hydrogen bonds. Dimensional fidelity assessed by microscopy imaging shows less than 2% shrinkage through the molding process and the water contact angle is approximately 80°. As there is generally little absorption of UVA light (365 nm) in proteins and nucleic acids, this UVA-bonding procedure should be applicable for packaging a wide variety of biosensors into lab-on-a-chip systems.

Keywords: Biocompatible bonding, silicon biosensor, silicon-polymer integration, off-stoichiometry-thiol-ene-epoxy, lab-on-a-chip, microfluidic packaging.

IOP Publishing Journal Title
Journal **XX** (XXXX) XXXXXX https://doi.org/XXXX/XXXX

1 Introduction

Recent progress in lab-on-a-chip (LOC) technology unveils an increasing interest and need for integration of several subcomponents, often manufactured in different materials, into one functional system (Andreassen and Mielnik, 2014; Chen et al., 2021; Dornhof et al., 2022; Lindsay et al., 2018; Mielnik et al., 2013; Valera et al., 2016). In many respects, the idea of realizing monolithic systems (system-on-chip) is being abandoned, gradually shifting towards a more heterogeneous (system-in-package) approach. This shift is fueled by applications which require ever more functional systems, like novel diagnostic devices comprising biosensors and microfluidics, and the acknowledgement that no single material or fabrication technology alone can fulfill all needs.

A large group of biosensors are those where the transducer is manufactured by silicon micro- and nanofabrication technologies (Luan et al., 2018; Poghossian and Schöning, 2021). Packaging of such biosensors into LOC devices is particularly challenging since the transducer must be functionalized with a biorecognition molecule to complete the biosensor. If packaging is performed as the first step, i.e., prior to biofunctionalization, it limits the multiplexing capabilities and substantially complicates the biofunctionalization procedure (Leichlé et al., 2012). Biofunctionalization prior to biosensor packaging, on the other hand, poses challenging process requirements; the packaging must not compromise the biological activity of the attached biomolecules. This means that most standard microfabrication bonding techniques, which typically require high temperatures, non-biocompatible chemicals, or plasma activation (Taklo, 2002), are not applicable (Leichlé et al., 2012; Lepock et al., 1993). These packaging challenges are substantially limiting the adoption of biosensors into commercial utilization in novel diagnostic devices.

Common methods for biocompatible biosensor packaging[1] in research include clamping of microfluidic structures either molded in soft materials like polydimethylsiloxane (PDMS) or cut in polymer sheets like Mylar (Washburn et al., 2010). Application of pressure sensitive adhesives to bond structured polymer (e.g., cut or milled) onto the biosensor die (Kratz et al., 2019) is another common approach. Cutting or milling microfluidic structures from polymer sheets drastically limits design opportunities, and clamping solutions are prone to leakage. To fully exploit the potential of microfluidics to enhance the performance of LOC systems, the package fabrication process should allow integration of complex micro- and nanofluidic patterns. This is feasible with PDMS molding, but the material possesses several intrinsic properties that complicate its use in LOC systems. Examples are absorption of small hydrophobic molecules and high gas permeability causing gas bubble formation and evaporation over the time course of an experiment (Sticker et al., 2015). Another important downside of PDMS is that high volume production and commercialization are hindered by up-scaling difficulties and low fabrication throughput (Volpatti and Yetisen, 2014).

Another group of moldable polymers utilized for microfluidic applications are thiol-enes (Bartolo et al., 2008; Bong et al., 2012), off-stoichiometry thiol-enes (referred to as "oste" in many publications) (Carlborg et al., 2011; Pardon et al., 2014; Saharil et al., 2012) and off-stoichiometry thiol-ene-epoxies (referred to as "oste+" in many publications) (Carlborg et al., 2014; Sandström et al., 2015; Sticker et al., 2015), solving some of the challenges of PDMS. They offer e.g., direct dry-bonding to surfaces like silicon and glass, low gas permeability, tuneable mechanical properties from rigid to rubbery states, tuneable surface properties with permanent surface modifications, and are compatible with both prototyping and medium-scale volume manufacturing. For a closer description of off-stoichiometry thiol-ene and off-stoichiometry thiol-ene-epoxy polymers, see Haraldsson et al. (2014) and the references above.

Off-stoichiometry thiol-ene-epoxies are particularly useful for LOC technology as they are cured in two stages first forming a soft mold replicate, which after alignment to a substrate is cured to form a rigid bonded polymer. However, most work with this type of polymer including the commercially available resins ("OSTEMER 322 Crystal Clear," n.d., "OSTEMER 324 Flex," n.d.) perform bonding at non-biocompatible temperatures. In the work by Zhou et al. (2017), an off-stoichiometry thiol-ene-epoxy resin was used to mold and then UVA-bond a polymer well-array to a biofunctionalized microarray glass slide at room temperature. As the resin formulation is not given, replication to assess its applicability for silicon biosensor packaging is not possible.

In this work we use the commercially available off-stoichiometry thiol-ene-epoxy resin Ostemer 322 Crystal Clear (Mercene Labs, Sweden) and demonstrate a novel processing approach to obtain biocompatible packaging of a silicon biosensor into a lab-on-a-chip device. We discuss the fabrication process in detail, assess the physical properties of the device, and explore in particular how storage time between the first (thermal) curing step and the bonding step (UVA

[1] In the context of the present work, "biocompatible biosensor packaging" refers to the integration of a biosensor with microfluidics in a manner which does not deteriorate or corrupt the functionality of antibodies bound to the biosensor surface.

cure) affects the bonding strength of the silicon-polymer package. The latter is an important aspect for convenient use of pre-fabricated devices as well as for commercial utilization. Finally, we apply the packaging approach to antibody-functionalized silicon ring resonator sensors and assess its biocompatibility by running an antigen capture assay after packaging.

2 Materials and methods

2.1 Fabrication

2.1.1 Polymer chip

The polymer microfluidic cartridge was fabricated in the two-component resin Ostemer 322 Crystal Clear (oste322) (Mercene Labs, Sweden). Note that in the fabrication process we have developed the order of the two curing steps of this resin is reversed compared to the procedure provided by the manufacturer. The fabrication and packaging principle is illustrated in figure 1. The starting point is two positive molds milled in PMMA (figure 1a,c) from which negative PDMS molds (figure 1b,d) are cast before assembling them to a PDMS reaction injection mold (figure 1e) used to fabricate the polymer microfluidic cartridge (figure 1f). Details on the fabrication of PMMA and PDMS molds are found in the Supplementary Information (section S1). Milled PMMA was used as fabrication master due to the relatively large depths of the chip's features. PDMS was used as an intermediate molding step due to its superior de-bonding properties from oste322 as compared to PMMA, mainly attributed to its mechanical flexibility and low oste322 adherence.

The polymer microfluidic cartridge (figure 1f-g) was designed with 3 microfluidic channels (500 µm wide, 100 µm deep). The cartridge has an area of 14 mm x 29 mm and thickness 600 µm. Structures for the direct coupling of external tubing to the microfluidic cartridge – two tube connector arrays – were integrated into the design (thickness 3 mm, area 5.2 mm x 14 mm, inlet holes 2.4 mm diameter). This gives a total polymer thickness of 3.6 mm (3 mm plus 600 µm) at the position of the tube connector arrays.

Oste322 component A and B were mixed in weight ratio 1.09:1 by vortexing in a 30 ml glass vial and left on the bench to evacuate air-bubbles. PDMS mold 1 (figure 1b) and 2 (figure 1d) were aligned to make the reaction injection mold (figure 1e). Due to the relatively large contact area between the two PDMS molds, they adhere sufficiently well to each other without the need for additional mechanical clamping during the subsequent pre-polymer injection and thermal cure. Up to four molds were used in parallel to fabricate four microfluidic cartridges simultaneously. The oste322 pre-polymer was injected using a 5ml luer-slip syringe, also filling the mold's inlet and outlet holes (figure 1e). These will serve as backfilling reservoirs as the oste322 slightly contracts during the first cure (Sandström et al., 2015). The assembly was baked in an oven at 90°C until the liquid oste322 pre-polymer had become a solidified but soft material. The time to reach solidification varied between the oste322 batches from 1.5 hours to 5.5 hours. To evaluate the onset of solidification without opening the reaction injection mold, a simple PDMS mold with a 1 mm deep cavity (size of a standard microscope slide) was used in parallel. In this mold, oste322 pre-polymer was poured into the cavity and covered with a release liner (Fluoropolymer coated release liner 9755, 3M™ Scotchpak™). After the thermal cure, the assembly was completely cooled down before carefully demolding PDMS mold 2. The oste322, still attached to PDMS mold 1, was placed in a holder milled in PMMA (supplementary figure S1). Before transfer the areas of the holder to be in contact with oste322 were covered with release liner. PDMS mold 1 was carefully removed and excess oste322 cut away with a scalpel leaving only the structure of the final polymer microfluidic cartridge (figure 1f). After this, the oste322 cartridge was either bonded to the silicon chip at once, or it was covered with release liner and stored at room temperature protected from light for 1, 2, 4 and 18 weeks prior to bonding to assess the suitability for storage of prefabricated oste322.

2.1.2 Silicon chip

To assess the biocompatibility of the packaging procedure, ring resonator sensors were fabricated on silicon-on-insulator wafers, biofunctionalized with antibodies and covered with DryCoat (Virusys Corporation) before bonding. The chips were 14 mm by 29 mm with a ring resonator layout matching the microfluidic channel design of the polymer cartridge. The design and fabrication of the ring resonator sensors, biofunctionalization procedure and application of DryCoat are described in detail in the Supplementary Information (section S3).

In addition, non-structured silicon chips (blank chips) were prepared for assessment of bonding strength. Silicon wafers (⟨100⟩ 675 µm thickness, Topsil) were thermally oxidized (7615 Å) before dicing (14 mm x 29 mm chips). Directly before bonding to oste322 the blank silicon chips were cleansed by ultrasonication for 5 min in acetone, then isopropanol, then deionized water, rinsed 3 times in deionized water and blown dry with dry filtered air.

2.1.3 Bonding

The bonding and the second curing step of oste322 happens simultaneously (1f-g). The silicon chip was aligned to the thermally cured oste322 held in the PMMA holder. The assembly consisting of the silicon chip, the oste322 and the release liner was lifted from the holder, and air-bubbles were removed by applying pressure with a blunt tool on top of the protective release liner on the oste322. No clamping between the oste322 and silicon chip was necessary to retain surface contact during UVA exposure. Release liner pieces on the tube

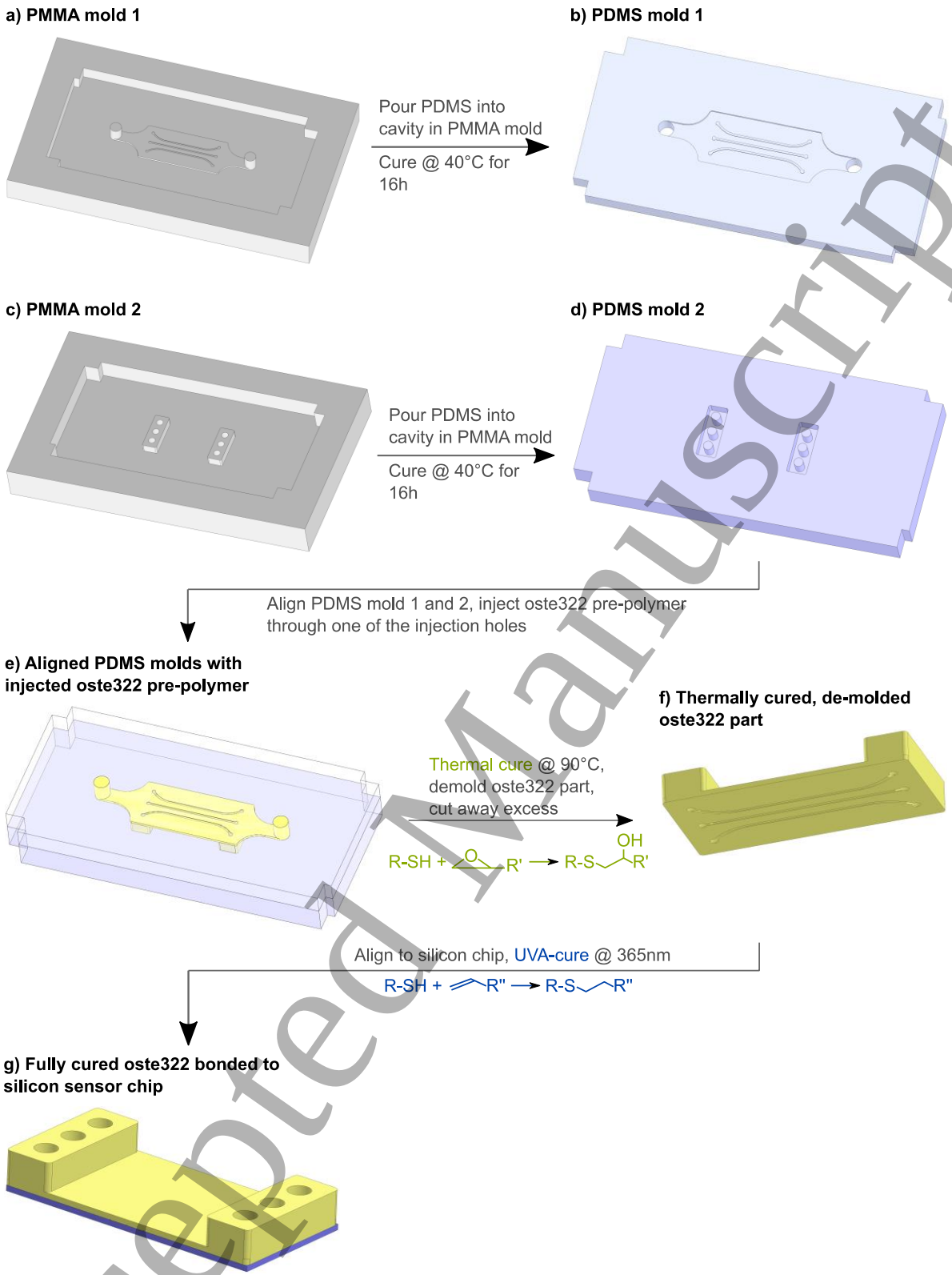

Figure 1: Fabrication procedure (a-g) Schematic illustration of the fabrication procedure developed to mold and then biocompatibly UVA-bond oste322 microfluidic cartridges to silicon sensor devices. (a,c) Positive molds are milled in PMMA. (b,d) Negative PDMS molds are cast from the PMMA-molds. (e) The PDMS molds are assembled to form a reaction injection mold and oste322 pre-polymer is injected before a thermal cure at 90°C where thiol and epoxy groups react. (f) The soft intermediate oste322 is demolded, excess structures from the molding process are cut away, (g) the oste322 is aligned to the silicon sensor and UVA light initiates the second cure where thiol and allyl groups react, resulting in a rigid polymer which is bonded to the silicon sensor chip. Details of the fabrication procedure are found in section 2.1.

connector arrays were removed before exposure to UVA-light (Dymax light curing systems, model 1200 focused beam, UVA-range intensity (320-390 nm) 350 mW/cm2) for 2 x 2 sec with 20 sec pause between exposure steps with aluminum foil covering the 0.6 mm thick part of the oste322. The aluminum foil and last release liner piece were removed to expose the entire oste322 device for an additional 2 x 2 sec with a 20 sec pause. This gave a total of 8 sec UVA exposure for the 3.6 mm thick part and 4 sec for the 0.6 mm thick part to fully cure and bond all parts of the device while not overexposing.

For the biofunctionalized ring resonator chips, the DryCoat was removed by immersion in deionized water before oste322 bonding. After bonding, DryCoat was injected into the microfluidic channels, incubated for 1 min, and removed before further storage at 4°C. To assess the effect of the bonding procedure on antibody function, one un-functionalized ring resonator chip was bonded to oste322. On this chip the biofunctionalization (section 2.1.2) and antigen capture assay (section 2.3) were performed in one continuous run.

2.2 Physical characterization

The bonding strength between the silicon chip and polymer microfluidic cartridge was determined in terms of static liquid pressure with a set-up as illustrated in supplementary figure S2. A syringe pump (Harvard Apparatus PHD2000) was connected to the inlet, while a pressure sensor (GD4200, ESI Technology Ltd) was connected to the outlet of a channel in the silicon-polymer package. Deionized water was filled into the silicon-polymer package before connecting the pressure sensor. The syringe pump was run at constant flow rate between 200 and 500 µl/min while using a stereomicroscope with a large field of view covering the entire silicon-polymer package for optical monitoring of leakage. In addition to real-time visual inspection, images were acquired throughout the experiments and digitally analysed to identify potential minor leaks. All packages were tested up to 500 mbar, while a selection was tested to 2500 mbar (overview in table 1). Up to 500 mbar the silicon polymer package was connected by PTFE-tubing (ID: 0.3 mm, OD: 1.6 mm, VWR) with a silicone tubing sleeve (ID: 1.02 mm, OD: 2.16 mm, VWR), inserted into the inlet holes in the tube connector arrays. Above 500 mbar gluing was necessary to achieve a leak-tight connection between chip and tubing. All pressure values refer to gauge pressure.

Topographical measurements of PMMA mold 1 and the oste322 bond surface (after bonding) were done using white light interferometry (WYKO NT9800, Veeco). Arithmetic average surface roughness, R_a, was calculated by:

$$R_a = \frac{1}{n}\sum_{i=1}^{n}|Z_i - \bar{Z}| \quad (1)$$

where Z_i is the vertical height of grain i and $\bar{Z}$ the average grain height. Reported values for R_a (average ± standard deviation), in addition to average and maximum peak-to-valley roughness, are based on analyzing in total 5 mm x 6.8 mm of the surfaces.

The water contact angle was measured by pipetting 40 – 180 µl deionized water on the top surface of the polymer microfluidic cartridge, imaging and measuring the left and right contact angles.

Dimensional fidelity in the two-step molding process was assessed by fabrication of an oste322 device with integrated herringbone mixing structures in the upper microfluidic channel wall. To fabricate this device, we used a photolithography defined SU-8 mold to define the microfluidic structures and a milled PMMA mold to define the outer dimensions of the microfluidic cartridge. Fabrication of this cartridge is described in the Supplementary Information (section S5). Replication of microstructural dimensions from the SU-8 mold to PDMS mold to oste322 cartridge was assessed by microscopy imaging and image analysis. Dimensional fidelity assessment was performed on this device instead of the previously described oste322 cartridge as accurate comparison of dimensions are better allowed by the fine photolithography patterns and accurate dimensional replication is crucial for the function of such mixing structures.

All imaging was performed using an Olympus SZX10 stereomicroscope (assessing bonding strength and contact angle) or Olympus BX-61 microscope (assessing dimensional fidelity), Olympus XM10 camera and cellSens Dimension software (Olympus) for image analysis.

2.3 Biocompatibility of the packaging procedure

To assess the biocompatibility of the packaging procedure, antibody-functionalized ring resonator sensors were packaged (described in section 2.1) prior to running an antigen capture assay in the LOC devices. The experimental set-up is illustrated in figure 2. For optical characterization, a tapered lensed fiber with 14 µm working distance and 2.5 µm spot diameter was used to couple light into the waveguide. A tunable external cavity laser (Thorlabs TLK-L1550M) with 1550 nm center wavelength was used as the light source. A fiber polarization controller (Thorlabs FPC562) was placed between the light source and the tapered fiber to control the input polarization of the light. A single mode fiber connected to InGaAs photodetectors (Thorlabs DET10C2) was placed in front of the output waveguide to capture the output power from the resonators. For fluidic operation, a syringe pump (Harvard Apparatus Pump 11 Pico Plus Elite) in withdraw mode was used. The syringe pump and reagent vials were connected to the LOC device by PTFE-tubing with a silicone tubing sleeve. The antigen capture assay was performed as follows at flow rate 20 µl/min; 1) 5 min buffer, 2) 15 min 5 µg/ml CRP (control antigen, C-reactive protein, SigmaAldrich) in buffer, 3) 5 min buffer, 4) 20 min 5 µg/ml

Vtg (target antigen, Vitellogenin, Biosense Laboratories) in buffer, 5) 5 min buffer ("buffer" = PBS (phosphate buffered saline, SigmaAldrich) with 5 mg/ml BSA (bovine serum albumin, SigmaAldrich)). Small deviations to the time length of each step occurred due to fluidic operation considerations. During the antigen capture assay the laser was scanned across the selected resonance, and wavelength vs power for each sweep was stored in a separate file with the time stamp. After the measurements, Lorentzian fitting was performed on each wavelength sweep to extract the information about the resonance wavelength. Resonance wavelengths were then plotted against time stamps.

3 Results and discussion

3.1 Fabrication procedure

In this work we have used the commercial polymer Ostemer 322 Crystal Clear (oste322) (Mercene Labs, Sweden) and processed it in a novel manner to obtain biocompatible packaging of a silicon biosensor into a lab-on-a-chip device. Oste322 is a two-component resin, an off-stoichiometry thiol-ene-epoxy made specifically for the requirements of microfluidics, MEMS and lab-on-a-chip ("OSTEMER 322 Crystal Clear," n.d.). As opposed to PDMS it is slightly hydrophilic (Sandström et al., 2015) and has low water vapor permeability (Sticker et al., 2015). Fabrication of devices rely on a two-step polymerization reaction where the liquid pre-polymer solidifies to a soft intermediate state replicating the mold structure in the first curing step initiated by UVA light (365 nm). The oste322 is then demolded and aligned to the substrate before the second curing step initiated by heat (90 – 110°C). This makes the polymer rigid like typical thermoplastics and simultaneously covalently bonded to the substrate ("OSTEMER 322 Crystal Clear," n.d.). Since this last curing step where the oste322 device bonds to the substrate takes place at 90-110°C, it is not appropriate for packaging biofunctionalized sensors as the biomolecules would denature. There is little absorption of UVA light at 365 nm in proteins and nucleic acids (de Gruijl, 2000; Porterfield and Zlotnick, 2010; Rastogi et al., 2010; Ravanat et al., 2001). Therefore, we hypothesized that we could obtain a biocompatible LOC packaging procedure if we were able to achieve proper curing and bonding of oste322 when reversing the order of the two curing steps.

When reversing the curing order (reverse cure) compared to that specified by the manufacturer (standard cure), finding appropriate thermal curing conditions required comprehensive experimentation. Differences between oste322 batches from the manufacturer complicated the matter, but there was consistency within batches. We concluded that the best approach for the thermal cure was to always use 90°C temperature and adapt the curing time for each oste322 batch. We found the curing times to be independent of oste322 device thickness. We achieved similar end results for all oste322 devices when utilizing this approach. Whether the first cure was a thermal or UVA cure, the physical appearance of the oste322 was similar; a soft, slightly sticky intermediate state with softness resembling cured PDMS. During storage of the thermally cured oste322 protected from light for up to 18 weeks the material gradually became less sticky and less soft.

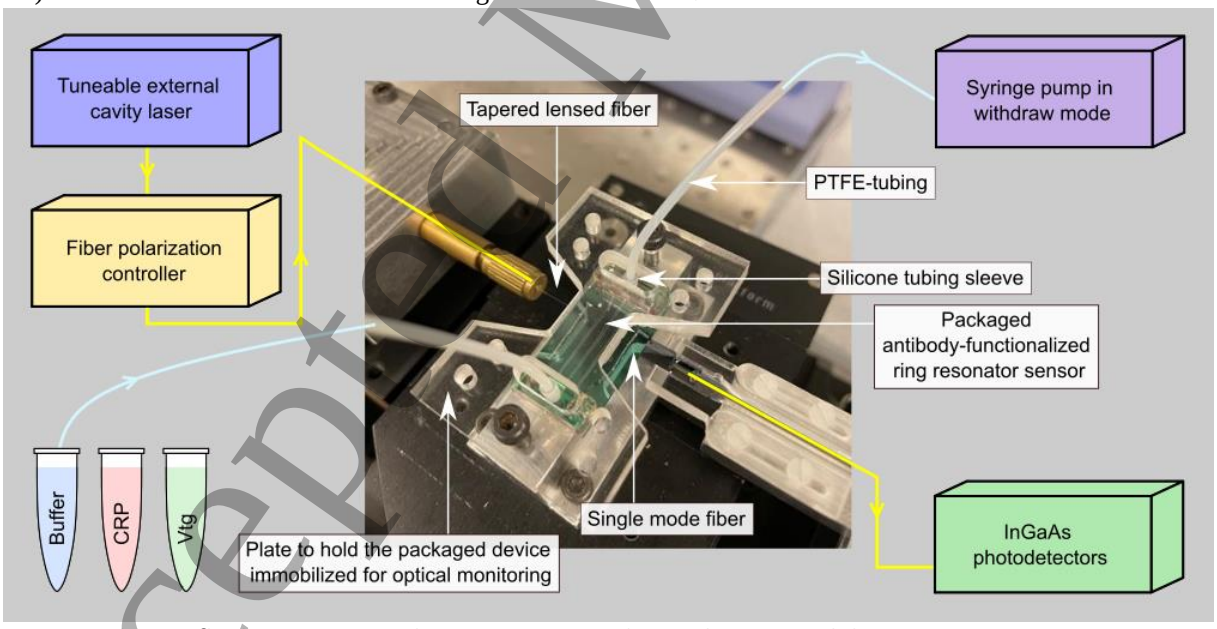

Figure 2: Optical-microfluidic experimental set-up to test packaging biocompatibility The set-up was used to test the antibody functionalized ring resonator sensors that were packaged with the polymer microfluidic cartridge. The reagents of the antigen capture assay were pumped through the microfluidic channel during continuous optical monitoring of the sensor response to record binding events on the sensor surface, to assess the biological function of the antibodies after packaging. The yellow and light blue lines illustrate the optical and fluidic pathways, respectively. The experimental procedure is described in section 2.3.

The stickiness faded most rapidly, and after four weeks the oste322 was no longer sticky. The softness gradually decreased, but even after 18 weeks the oste322 was still soft enough to easily bend and adhere to the silicon chip surface.

The UVA cure could be performed with the same UVA exposure regime for all batches of oste322. The appropriate regime was found by performing the UVA cure as the first cure and exposing 2 seconds at a time until the pre-polymer solidified. Using reaction injection molds was very useful for these experiments as the oste322 device thickness was constant, and the appropriate UVA dose depends on oste322 thickness. Since the oste322 device has one area with thickness 0.6 mm and two areas with thickness 3.6 mm, they were exposed for different times to avoid overexposure of the thin area. The exposure was divided into repeating intervals of 2 seconds exposure followed by 20 seconds pause since the UVA-initiated reaction is exothermic ("Datasheet Ostemer 322 Crystal Clear," 2019). If measures are not taken to limit the temperature increase during this exothermic reaction, this step might also cause thermal denaturation of the antibodies bound to the sensor surface. We found that separating the total exposure time in intervals of 2 seconds with 20 seconds resting time between exposures sufficiently reduced the heat generation to avoid antibody denaturation. If working with biosensors functionalized with more temperature-sensitive biomolecules, the silicon-polymer package may be cooled down while performing the UVA exposure.

After both curing steps of the reverse cure, the oste322 physical appearance is the same as after the full standard cure; it is hard and rigid like a typical thermoplastic. However, the bonding characteristics are different. Whereas the standard curing order results in a silicon-polymer package which is covalently bonded together, the reverse curing order results in a package which may be de-bonded after use (figure 3a-b). Although de-bondable, the reverse cured packages withstand more than 2500 mbar of fluidic pressure (see section 3.2.1), more than enough for most microfluidic applications. This combination of properties is very useful in LOC research as the silicon sensor die may be re-used or inspected with techniques requiring free access to the surface.

The reason for the difference in bonding properties for the standard and reverse cure is the chemical formulation of the resin. Oste322 contains 3 different monomers, each with either a thiol, allyl or epoxy functional group (monomers illustrated in figure 1e-g). In the standard cure, the first cure initiated by UVA light causes thiol and allyl functional groups to react, and the second cure initiated by heat causes thiol and epoxy functional groups to react (Sandström et al., 2015). The covalent bonding of oste322 to silicon during the thermal cure is caused by the epoxy groups forming covalent bonds to hydroxyl groups on the silicon / silicon oxide surface ("Datasheet Ostemer 322 Crystal Clear," 2019). When reversing the curing order, the bonding curing step is the one

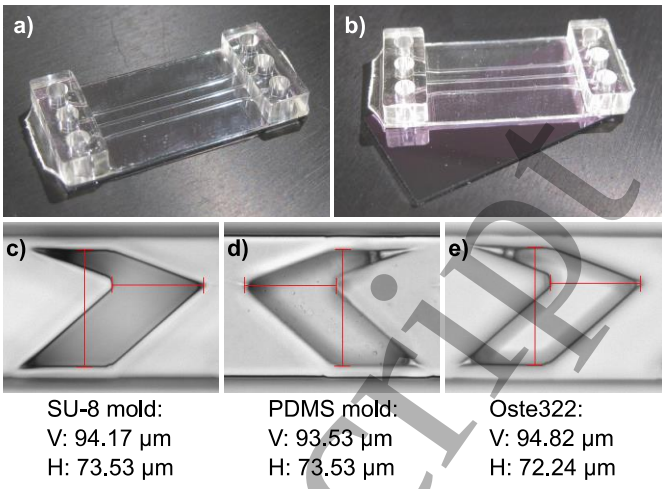

Figure 3: Final silicon-polymer package and dimensional fidelity assessment (a) Image of the final bonded silicon-polymer package. (b) Image of the silicon-polymer package after de-bonding. (c-e) Dimensional fidelity throughout the two-step molding process from the SU-8 mold to PDMS mold to oste322 was assessed by measurement of the vertical (V) and horizontal (H) red lines in the microscope images. The width of the mixing pattern (vertical line; approximately 94 µm) is smaller than the mask design of 100 µm due to the double-layer SU-8 photolithography process.

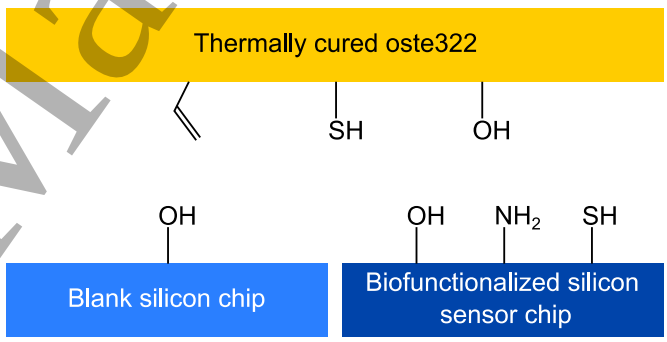

Figure 4: Surface functional groups Schematic illustration of the surface functional groups on the different bonding surfaces. After the thermal cure, the oste322 surface contains allyl, thiol and hydroxyl functional groups. The blank (i.e. non-structured and non-biofunctionalized) silicon chips have hydroxyl functional groups, forming hydrogen bonds with hydroxyl and dipole-dipole interactions with thiol on oste322. Biofunctionalized silicon sensor chips are blocked with BSA protein where various amino acid side chains introduce various functional groups. Hydroxyl (serine, threonine, tyrosine) and nitrogen-containing (asparagine, glutamine, histidine) functional groups (here illustrated through a primary amine) are mainly responsible for hydrogen bonding at neutral pH to hydroxyl on oste322. Thiol (cysteine) may potentially form covalent bonds with thiol (disulphide bridges) and allyl (UVA-initiated reaction) on thermally cured oste322. In addition dipole-dipole interactions are possible for many amino acid side chains with thiol and hydroxyl on oste322 (not illustrated).

initiated by UVA where thiol and allyl groups react. None of these functional groups form covalent bonds with hydroxyl groups on the silicon substrate. However, the thermal cure reaction of thiol and epoxy results in a product containing a hydroxyl group (figure 1e-f) (Sandström et al., 2015). Hence, the thermally cured oste322 aligned to the silicon chip contains thiol, allyl, and hydroxyl functional groups before the UVA cure. Both for the blank (i.e., non-structured and non-biofunctionalized) and the biofunctionalized ring resonator chips the functional groups on the surfaces enable hydrogen bonding and dipole-dipole interactions with the thermally cured oste322 (figure 4). These intermolecular forces only become significant when the involved molecules are physically close together. Since the oste322 is soft and adheres well to the silicon chip, it may conform to the silicon surface topography maximizing intermolecular forces. This is supported by the surface roughness measurements described in section 3.2.1. The slight heat generation caused by the exothermic reaction might assist this action. As the oste322 stiffens after replicating the silicon surface topography, the bonding is also likely enhanced simply by frictional forces. The surface of the blank silicon chips only has hydroxyl functional groups. For the biofunctionalized ring resonator chips the whole surface is covered with BSA protein where the various amino acid side chains introduce several functional groups. By that, the blank silicon chips only enable intermolecular forces, while the biofunctionalized ring resonator chips might also facilitate covalent bonds; since thiol and allyl groups of oste322 react in the UVA cure, allyl groups on oste322 may likely also react with cysteine thiol groups on biofunctionalized sensors, forming covalent bonds. In addition, as there are thiol groups on both the oste322 and the biofunctionalized sensors, there is potential for formation of disulphide bridges.

The bonding of the surfaces by mainly intermolecular forces with a large extent of hydrogen bonds fits well with the observed bonding characteristics. Although intermolecular, when hydrogen bonds are formed over a large area, they become truly significant. This is exemplified e.g., by the DNA double helix (Watson and Crick, 1953) and its great structural stability, combined with the unwinding functionality. Also, as close surface proximity is obtained and there are hydroxyl groups on all bonding surfaces, the bonding mechanism between oste322 and silicon chips likely resembles the pre-bonding step of fusion bonding of hydrophilic silicon wafers (Taklo, 2002), exhibiting similar characteristics.

3.2 Physical characterization

3.2.1 Bonding strength

An overview of the results from investigating the bonding strength between the silicon chip and polymer microfluidic cartridge is found in table 1. All the silicon-polymer packages were tested up to 500 mbar while a selection was tested up to 2500 mbar (gauge pressure). No sign of leakage was observed in any of the tests. The packages could be de-bonded after use, leaving a clean silicon surface (figure 3a-b). The bond strength tests demonstrate a shelf life of more than 18 weeks between microfluidic cartridge molding and cartridge-to-silicon bonding – a significant advantage for both commercial utilization and research projects. With microfluidic cartridges in stock, the biofunctionalized silicon sensors may be packaged in minutes when ready to perform a bioassay experiment. During storage, the microfluidic cartridges were

Table 1: Bonding strength characterization Overview of experimental parameters (light grey) and results (dark grey) for the characterization of bonding strength between the silicon chip and polymer microfluidic cartridge. Experiments were performed with two technical replicates.

Silicon chip type	*Oste322 stored on release liner*	*Storage time*	*Tolerates 500 mbar*	*Tolerates 2500 mbar*
Blank	No	No storage	Yes	Not tested
Blank	Yes (contacted)	No storage	Yes	Yes
Blank	Yes	1 week	Yes	Not tested
Blank	Yes	2 weeks	Yes	Not tested
Blank	Yes	4 weeks	Yes	Yes
Blank	Yes	18 weeks	Yes	Yes
Biofunctionalized ring resonator chip	No	No storage	Yes	Yes

covered by release liner to avoid dust accumulation. As evidenced by the bond strength measurements, contact with release liner does not deteriorate the bonding properties of oste322 to an extent that affects the application, i.e., the bond strength of at least 2500mbar is maintained.

The arithmetic average surface roughness of the master PMMA mold 1 was R_a = 0.02 ± 0.09 µm while the corresponding bonding surface of oste322 had R_a = 0.02 ± 0.02 µm. 3D surface plots are found in supplementary figure S4. By that, the variation in surface topography is larger in the master mold than in the oste322 product. Average and maximum peak-to-valley roughness was 0.26 µm and 62 µm for PMMA mold 1, and 0.11 µm and 8 µm for oste322, respectively. These maximum peak-to-valley values originate from small areas with scratches in PMMA mold 1. As evidenced by the difference between the average and maximum values, they are not representative of the bonding surfaces. As discussed in section 3.1, the oste322 is soft when adhered to the silicon chip and may therefore conform to the very flat silicon surface, reducing the surface roughness and increasing the contact area for bonding. This increases the applicability of the bonding procedure, as cost-efficient molds which often have rougher surface topography may be utilized.

The measurement range of our experimental set-up was limited to 2500 mbar fluidic pressure. As all packages withstood this pressure level we were not able to assess differences in bonding strength for packages with biofunctionalized ring resonator chips and blank silicon chips. From the theoretical possibilities of bond formation discussed in section 3.1, it would be interesting to test whether biofunctionalized ring resonator chips tolerate higher pressures, as they feature the possibility of covalent bonds (thiol – allyl, thiol – thiol), in addition to intermolecular bonds available for both types of chips. However, as also the biofunctionalized ring resonator packages may be de-bonded after use, this implies that covalent bonding, if present, is not the dominant bonding mechanism.

3.2.2 Contact angle

The contact angle of deionized water with the reverse cured oste322 was found to be approximately 80° (ranging from 73° - 85°). Sandström et al. (2015) reported a water contact angle of 67° for standard cured oste322, while Zhou et al. (2017) reported 70 ± 3° using 4 µl droplets of deionized water. The slight increase in contact angle in our experiments could indicate that reversing the curing order slightly increases the water contact angle. However, conclusions are difficult as the contact angle measurements are affected by droplet size, surface roughness and image analysis. Nevertheless, for both the standard and reverse cured oste322, the water contact angle is in the same range – on the slightly hydrophilic side.

3.2.3 Dimensional fidelity

A valuable feature for LOC biosensors is the integration of microfluidic structures for advanced flow manipulation. One example is the integration of passive mixing structures to enhance the mass transfer of analyte to the sensing area (Oevreeide et al., 2021a, 2021b). Feature dimensions are essential for such microfluidic structures. We therefore assessed the dimensional fidelity throughout the two-step molding process for fabrication of such a device. To fabricate the passive mixing structures, the microfluidic geometry was defined by SU-8 photolithography instead of milling. Investigation of dimensions in the photolithography defined SU-8 mold, PDMS mold and oste322 device (figure 3c-e) shows that dimensions are transferred through the two replication processes with less than 2% shrinkage. Low shrinkage from the SU-8 mold to the PDMS mold is attributed to PDMS curing at low temperature (40°C) (Madsen et al., 2014). Our results correspond well with the work of Sandström et al. (2015) who demonstrate less than 1% shrinkage with oste322 standard cure for structures with comparable dimensions. This indicates that reversing the cure order does not significantly affect shrinkage. We expect similar dimensional fidelity for the PMMA to PDMS to oste322 molding process.

3.3 Biocompatibility of the packaging procedure

To investigate if the biological function of the antibodies was maintained after packaging, antibody-functionalized ring resonator sensors were bonded to oste322 cartridges prior to running an antigen capture assay. The antigen capture assay included a control antigen and a target antigen to assess binding selectivity. The working principle of ring resonator biosensors is explained e.g., in Washburn et al. (2009). In short, when the antibody bound to the sensor surface binds to another molecule, a shift in the resonance wavelength is observed. A representative measurement from the antigen capture assay is shown in figure 5. When the buffer (5 mg/ml BSA in PBS) or 5 µg/ml control antigen in buffer is run through the channels, we see no resonance shift, indicating no binding. However, as the solution of 5 µg/ml target antigen in buffer is introduced, the resonance wavelength shifts by approximately 300 pm, indicating antigen binding.

In total, four experimental replicates were performed with ring resonator chips bonded to oste322 after biofunctionalization. In addition, one ring resonator chip was bonded to oste322 before biofunctionalization, performing the biofunctionalization assay and antigen capture assay in one continuous run in the microfluidic channel, as a reference. Thus, in the latter case, the antibodies were not exposed to the packaging procedure. For all experiments, a similar profile as seen in figure 5 was observed for the antigen capture assay, with the size of the resonance shift varying between approximately 300 and 400 pm. For the ring resonator chips biofunctionalized before oste322 bonding, the resonance

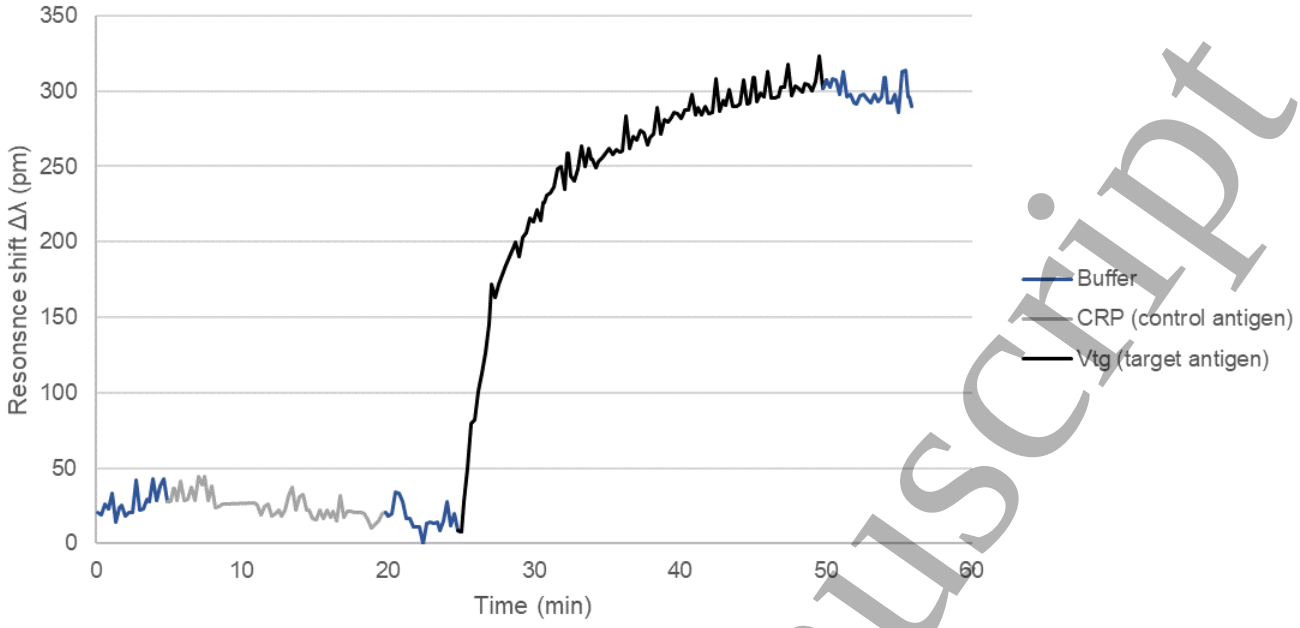

Figure 5: Test of the biocompatibility of the packaging procedure A plot showing the real-time monitoring of the shift in resonance wavelength (Δλ) of an antibody-functionalized ring resonator sensor after packaging as the different solutions of the antigen capture assay are run through the microfluidic channels, indicated along the time axis. "Buffer" = PBS with 5 mg/ml BSA, "CRP" = 5 µg/ml C-reactive protein in buffer, "Vtg" = 5 µg/ml Vitellogenin in buffer. The graph profile is representative for all experiments with the only difference being the size of the shift varying from approximately 300 – 400 pm.

shifts were 290, 290, 310 and 400 pm. For the ring resonator chip biofunctionalized after oste322 bonding, the shift was 330 pm. The observed variation in resonance shift between technical replicates is within expected levels and can be mainly attributed to the biofunctionalization procedure. It is known that, due to the small sensing area, batch-to-batch differences in number, orientation and monolayer formation of attached antibodies may cause significant differences in antigen capture ability (Arnfinnsdottir et al. (2020)), and hence resonance shifts. Therefore, data from ring resonator biosensors is commonly presented as averages over several technical replicates (Arnfinnsdottir et al., 2020; Graybill et al., 2016; Valera et al., 2016).

The resonance shift profiles indicate normal biological function of the antibodies with selective binding to the target antigen. The shift size is similar for antibodies which have been exposed to the packaging procedure and those which have not. This shows that the developed UVA-based packaging procedure is in fact biocompatible. There is in general little absorption of light at 365 nm in proteins and nucleic acids (de Gruijl, 2000; Porterfield and Zlotnick, 2010; Rastogi et al., 2010; Ravanat et al., 2001), and therefore we expect similar results for all such biorecognition molecules. By that, this packaging procedure should be applicable for packaging a variety of biosensors into lab-on-a-chip systems.

4 Conclusions

In this work, we have presented a new procedure which permits packaging of pre-biofunctionalized silicon sensors into a lab-on-a-chip system. We have shown that the packaging procedure does not compromise the biological function of the attached biomolecules. The polymer microfluidic cartridge is bonded to the silicon biosensors (as opposed to clamped) and can withstand pressures higher than 2500 mbar which far exceeds the typical pressure requirements for most LOC applications. This eliminates the widespread problem of leakage in clamped systems. Additionally, the bonding is reversible allowing disintegration of the microfluidic package for free access to the sensor surface or re-use of the silicon sensor.

The polymer cartridge is fabricated by reaction injection molding using oste322. When fully cured, it forms a rigid, slightly hydrophilic polymer (wetting angle approximately 80°) which has several advantages over the commonly used soft and hydrophobic PDMS. The fabrication process based on molding is suitable for upscaling, and it allows integration of complex microfluidic patterns permitting full utilization of the microfabrication design potential to enhance the performance of biosensor systems. In addition, the microfluidic cartridge may be stored for more than 18 weeks

before bonding, which drastically simplifies the logistics of the fabrication workflow.

In summary, this procedure overcomes many of the obstacles for microfluidic packaging of biosensors both for research and commercialization. By further developing this procedure for upscaled fabrication, we believe it could become an important contribution to the development and application of novel silicon biosensor-based diagnostic devices.

Acknowledgements

This work was supported by the Research Council of Norway through the Lab-on-a-chip Biophotonic Sensor Platform project (project number 248869/O70), and the Norwegian Micro- and Nano-Fabrication Facility, NorFab, (project number 295864). The funding source had no role in the present work. The authors declare that they have no conflicts of interests that could have appeared to influence the work reported in this paper. The authors gratefully acknowledge Jens Høvik and Dr. Jong Wook Noh at the Department of Electronic Systems, NTNU for building the Lab-on-a-chip optical characterization setup, Dr. Runar Dahl-Hansen at SINTEF Digital for performing the white light interferometry measurements, and the project consortium for fruitful discussions. Credit author statement: Linda Sønstevold: Conceptualization, Methodology, Investigation, Formal analysis, Visualization, Writing – Original Draft, Writing – Review & Editing. Mukesh Yadav: Investigation, Formal analysis. Nina Bjørk Arnfinnsdottir: Investigation. Aina Kristin Herbjørnrød: Investigation. Geir Uri Jensen: Methodology. Astrid Aksnes: Conceptualization, Writing – Review & Editing, Funding acquisition. Michal Marek Mielnik: Conceptualization, Investigation, Writing – Review & Editing, Supervision, Funding acquisition.

References

Andreassen, E., Mielnik, M.M., 2014. ESTC 2014 - 5th Electron. Syst. Technol. Conf. https://doi.org/10.1109/ESTC.2014.6962736

Arnfinnsdottir, N.B., Chapman, C.A., Bailey, R.C., Aksnes, A., Stokke, B.T., 2020. Sensors 20, 3163. https://doi.org/10.3390/S20113163

Bartolo, D., Degré, G., Nghe, P., Studer, V., 2008. Lab Chip 8, 274–279. https://doi.org/10.1039/B712368J

Bong, K.W., Xu, J., Kim, J.-H., Chapin, S.C., Strano, M.S., Gleason, K.K., Doyle, P.S., 2012. Nat. Commun. 3. https://doi.org/10.1038/ncomms1800

Carlborg, C.F., Haraldsson, T., Öberg, K., Malkoch, M., van der Wijngaart, W., 2011. Lab Chip 11, 3136. https://doi.org/10.1039/c1lc20388f

Carlborg, C.F., Vastesson, A., Liu, Y., van der Wijngaart, W., Johansson, M., Haraldsson, T., 2014. J. Polym. Sci. Part A Polym. Chem. 52, 2604–2615. https://doi.org/10.1002/pola.27276

Chen, X., Ning, Y., Pan, S., Liu, B., Chang, Y., Pang, W., Duan, X., 2021. ACS Sensors 6, 2386–2394. https://doi.org/10.1021/acssensors.1c00602

Datasheet Ostemer 322 Crystal Clear [WWW Document], 2019. URL https://www.ostemers.com/wp-content/uploads/2019/10/Data-sheet-OSTEMER-322-Crystal-Clear-v6.pdf (accessed 11.16.21).

de Gruijl, F.R., 2000. Methods Enzymol. 319, 359–366. https://doi.org/10.1016/S0076-6879(00)19035-4

Dornhof, J., Kieninger, J., Muralidharan, H., Maurer, J., Urban, G.A., Weltin, A., 2022. Lab Chip 22, 225–239. https://doi.org/10.1039/D1LC00689D

Graybill, R.M., Para, C.S., Bailey, R.C., 2016. Anal. Chem. 88, 10347–10351. https://doi.org/10.1021/acs.analchem.6b03350

Haraldsson, T., Carlborg, C.F., van der Wijngaart, W., 2014. Proc. SPIE 8976, Microfluid. BioMEMS, Med. Microsystems XII 8976, 897608. https://doi.org/10.1117/12.2041918

Kratz, S.R.A., Eilenberger, C., Schuller, P., Bachmann, B., Spitz, S., Ertl, P., Rothbauer, M., 2019. Sci. Rep. 9, 1–12. https://doi.org/10.1038/s41598-019-45633-x

Leichlé, T., Lin, Y.-L., Chiang, P.-C., Hu, S.-M., Liao, K.-T., Chou, C.-F., 2012. Sensors Actuators B Chem. 161, 805–810. https://doi.org/10.1016/J.SNB.2011.11.036

Lepock, J.R., Frey, H.E., Ritchie, K.P., 1993. J. Cell Biol. 122, 1267–1276. https://doi.org/10.1083/JCB.122.6.1267

Lindsay, M., Bishop, K., Sengupta, S., Co, M., Cumbie, M., Chen, C.-H., Johnston, M.L., 2018. IEEE Trans. Biomed. Circuits Syst. 12, 1046–1055. https://doi.org/10.1109/TBCAS.2018.2845867

Luan, E., Shoman, H., Ratner, D.M., Cheung, K.C., Chrostowski, L., 2018. Sensors 18, 3519. https://doi.org/10.3390/S18103519

Madsen, M.H., Feidenhans'l, N.A., Hansen, P.-E., Garnæs, J., Dirscherl, K., 2014. J. Micromechanics Microengineering 24, 127002. https://doi.org/10.1088/0960-1317/24/12/127002

Mielnik, M.M., Tofteberg, T.R., Andreassen, E., 2013. 17th Int. Conf. Miniaturized Syst. Chem. Life Sci. MicroTAS 2013 2, 796–798

Oevreeide, I.H., Zoellner, A., Mielnik, M.M., Stokke, B.T., 2021a. J. Micromechanics Microengineering 31, 015006. https://doi.org/10.1088/1361-6439/ABC820

Oevreeide, I.H., Zoellner, A., Stokke, B.T., 2021b. Micromachines 12, 556. https://doi.org/10.3390/MI12050556

OSTEMER 322 Crystal Clear [WWW Document], n.d. URL https://www.ostemers.com/products/ostemer-crystal-clear/ (accessed 11.16.21).

OSTEMER 324 Flex [WWW Document], n.d. URL https://www.ostemers.com/products/ostemer-flex/ (accessed 12.1.21).

Pardon, G., Saharil, F., Karlsson, J.M., Supekar, O., Carlborg, C.F., van der Wijngaart, W., Haraldsson, T., 2014. Microfluid. Nanofluidics 17, 773–779. https://doi.org/10.1007/s10404-014-1351-9

Poghossian, A., Schöning, M.J., 2021. Curr. Opin. Electrochem. 29, 100811. https://doi.org/10.1016/J.COELEC.2021.100811

Porterfield, J.Z., Zlotnick, A., 2010. Virology 407, 281–288. https://doi.org/10.1016/J.VIROL.2010.08.015

Rastogi, R.P., Richa, Kumar, A., Tyagi, M.B., Sinha, R.P., 2010. J. Nucleic Acids 2010. https://doi.org/10.4061/2010/592980

Ravanat, J.-L., Douki, T., Cadet, J., 2001. J. Photochem. Photobiol. B Biol. 63, 88–102. https://doi.org/10.1016/S1011-1344(01)00206-8

Saharil, F., Carlborg, C.F., Haraldsson, T., Van Der Wijngaart, W., 2012. Lab Chip 12, 3032–3035. https://doi.org/10.1039/c2lc21098c

Sandström, N., Shafagh, R.Z., Vastesson, A., Carlborg, C.F., van der Wijngaart, W., Haraldsson, T., 2015. J. Micromechanics Microengineering 25, 075002. https://doi.org/10.1088/0960-1317/25/7/075002

Sticker, D., Rothbauer, M., Lechner, S., Hehenberger, M.-T., Ertl, P., 2015. Lab Chip 15, 4542–4554. https://doi.org/10.1039/C5LC01028D

Taklo, M.M.V., 2002. Wafer bonding for MEMS. University of Oslo.

Valera, E., Shia, W.W., Bailey, R.C., 2016. Clin. Biochem. 49, 121–126.

https://doi.org/10.1016/J.CLINBIOCHEM.2015.09.001
Volpatti, L.R., Yetisen, A.K., 2014. Trends Biotechnol. 32, 347–350. https://doi.org/10.1016/J.TIBTECH.2014.04.010
Washburn, A.L., Gunn, L.C., Bailey, R.C., 2009. Anal. Chem. 81, 9499–9506. https://doi.org/10.1021/ac902006p
Washburn, A.L., Luchansky, M.S., Bowman, A.L., Bailey, R.C., 2010. Anal. Chem. 82, 69–72. https://doi.org/10.1021/ac902451b
Watson, J.D., Crick, F.H.C., 1953. Nature 171, 737–738. https://doi.org/10.1038/171737a0
Zhou, X.C., Sjöberg, R., Druet, A., Schwenk, J.M., van der Wijngaart, W., Haraldsson, T., Carlborg, C.F., 2017. Lab Chip 17, 3672–3681. https://doi.org/10.1039/C7LC00652G